# Design Optimization of Coreless Axial-flux PM Machines with Litz Wire and PCB Stator Windings

Murat G. Kesgin, *Student Member, IEEE*, Peng Han, *Member, IEEE*, Narges Taran*, *Member, IEEE*, Damien Lawhorn, *Student Member, IEEE*, Donovin Lewis, *Student Member, IEEE*, and Dan M. Ionel, *Fellow, IEEE*
SPARK Laboratory, ECE Dept., University of Kentucky, Lexington, KY, USA

murat.kesgin@uky.edu, peng.han@uky.edu, narges.taran@ieee.org,
damien.lawhorn@uky.edu, donovin.lewis@uky.edu, dan.ionel@ieee.org

***Abstract*—Coreless axial-flux permanent-magnet (AFPM) machines may be attractive options for high-speed and high-power-density applications due to the elimination of core losses. In order to make full use of the advantages offered by these machines and avoid excessive eddy current losses in windings, advanced technologies for winding conductors need to be employed to suppress the eddy effect, such as the Litz wire and printed circuit board (PCB). In this paper, the best practices for designing Litz wire/PCB windings are discussed and a brief survey of state of the art PCB winding technology is provided. Three coreless AFPM machines are mainly considered. A design optimization procedure based on the multi-objective differential evolution algorithm and 3-dimensional (3D) finite element analysis (FEA) is proposed to take into account the ac winding losses of Litz wires and PCB traces in the machine design stage. Selected designs are being prototyped and will be tested with a customized test fixture.**

***Index Terms*—Axial-flux, coreless, electric machine, multi-objective optimization, PCB, permanent magnet, Litz wire**

## I. Introduction

Coreless axial-flux permanent-magnet (AFPM) machines typically employ a special disk-type construction with a stator, which does not have a ferromagnetic core, positioned in between two rotors that ensure the magnetic return path. As a consequence, these machines may be, in principle, lighter and more efficient, because the stator core losses are eliminated [1]. Designs of coreless AFPM have been recently proposed and studied by the authors' extended research group [2]–[5] and by others, e.g. [6]–[8].

Because in a coreless machine the windings are directly exposed to the time-varying main magnetic field the eddy current losses in the stator conductors may be significant and special mitigation measures are required [9], [10]. Such constructive techniques include the use of special Litz wires, especially if the machines operate at high frequency [5], [11], [12].

An alternative approach is to employ printed circuit boards (PCBs) for the stator, such that copper traces serve as planar winding conductors between layers of laminated material. PCB stators have been reported as being compact, flexible, suitable for design modifications and accurate manufacturing techniques [13], and with good capabilities for heat dissipation [14].

A prototype motor for low-cost household applications was designed with a PCB stator employing a wave winding pattern and described in [13]. A non-overlapping concentrated winding with hexagonal concentric shapes was utilized in the PCB stator proposed in [14]. Multiple concentrated spiral-shaped winding variants were analyzed and a procedure for back electromotive force (EMF) calculation and PCB winding designs was proposed in [15]. A comparison of theoretical goodness predictions for wave windings [13] and hexagonal concentric patterns [14] led to the adoption of the wave winding pattern for the PCB stator design studied in the current paper.

## II. Coreless AFPMs with Litz Wire and PCB Stator Windings

Three coreless AFPM machines are considered for study (Fig. 1). Two-phase wave windings are used in the two machines shown in Fig. 1a and Fig. 1b to reduce the number of wire joints. Two-phase windings are advantageous in terms of balance. The minimization of the mutual coupling provides better fault tolerance. The third machine employs a special fractional-slot concentrated winding configuration, which is suitable to be fabricated with modular coil groups. All the machines are required to produce 12 Nm up to a speed of 3,000 r/min.

The higher the operating frequency is, the smaller the nominal single wire diameter has to be. To consider the interaction between several bundle diameters with skin depth, $\delta$, in a simplified way, the maximum single wire diameter is recommended to be smaller or equal to nearly $\delta/3$ [16].

The efficiency of coreless machines with PCB stators is heavily dependent on cross-sectional area of the copper traces. Reducing the conductor's height or width increases the dc copper loss due to lower current carrying capacity unless the number of tracks (turns) increases. Outside of a typical range, available copper trace height differs from manufacturer to manufacturer. The minimal copper trace width is limited by the precision of machines used in current manufacturing

*Dr. Narges Taran was with the SPARK Laboratory, ECE Department, University of Kentucky, Lexington, KY and is now with BorgWarner Inc., Noblesville Technical Center, IN, USA.

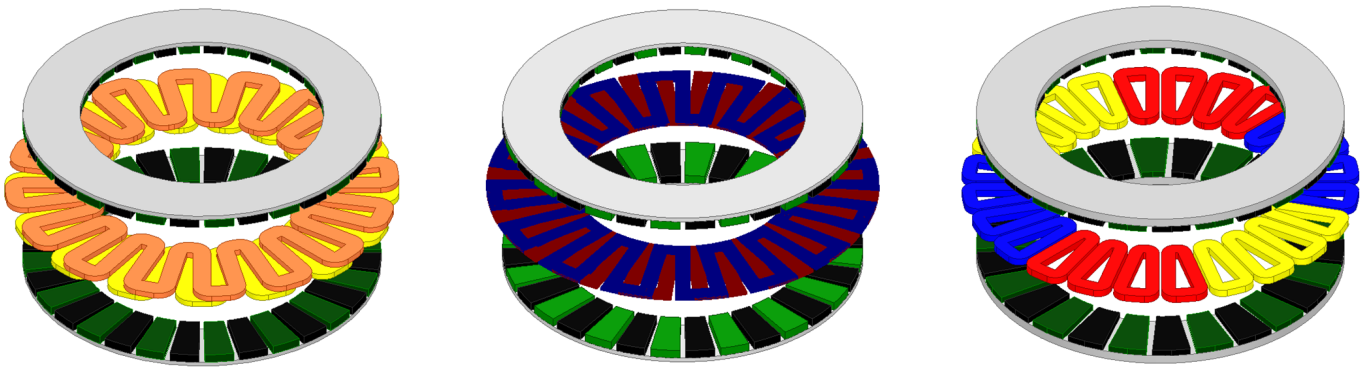

(a) (b) (c)

Fig. 1. Exploded views of coreless AFPM machines under study: (a) 2-phase AFPM with wave windings wound with Litz wires, (b) 2-phase AFPM with PCB wave windings, (c) 3-phase AFPM with fractional-slot concentrated windings.

practices. However, the number of traces can be increased axially by stacking and connecting more PCBs, creating more layers in the PCB, or by reducing the conductor width to allow for more traces on the same plane. Since higher numbers of printed boards increases the electromagnetic airgap, ideally, more traces should be placed on each single board.

The fill factor of PCBs is restricted by the material properties of the insulators between copper traces wherein voltage creepage threatens the integrity of the PCB if gaps are created below a minimum defined in current standards for PCB manufacturing. For a coreless machine operating at a very low fundamental frequency of 25 Hz, the copper trace width of 1.2 mm was employed [14]. Another group considered trace width of 0.2-0.3 mm and trace height of 0.07-0.105 mm with the gap between traces set at 0.23-0.3 mm for a machine operating at a fundamental frequency of 33.3 Hz [15]. In a PM machine designed for operation at 1 kHz, a copper trace width of 0.3 mm was adopted, with a 0.3 mm circumferential gap between traces [17]. The generic standard on PCB design, IPC-2221, recommends to have a minimum gap of 0.13 mm between traces at our intended voltage and a minimum trace width of 0.15 mm was chosen to allow for that gap for the design target under study.

## III. Estimation of Eddy Current Loss in Machine Windings

Litz wires consist of multiple strands insulated electrically from each other, which are usually twisted or woven to minimize the skin effect and proximity effect. Accurate predictions of eddy current loss in Litz wires involve detailed 3D wire models for which the scale of the problem is usually prohibitive for solving without using the high performance computing system. To reduce the burden of modeling and computation, numerous reduced-order methods were proposed, such as the fast 2.5-dimensional (2.5D) partial element equivalent circuit [18], the combined numerical and analytical approach called the squared-field-derivative method [19], the hybrid method that combines the analytical equations and FE simulations [9], [10], etc.

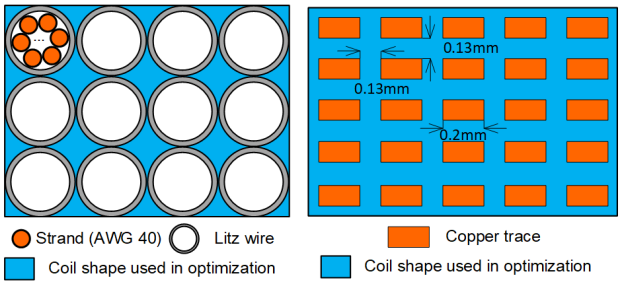


Fig. 2. Cross sections of equivalent macro coils of Litz wire and PCB stator windings used in 3D parametric models for optimization. Dimensions of PCB traces and the gap between them depend on the number of layers, overall thickness, finnished copper, etc., and are closely related to PCB manufacturers.

In contrast with Litz wire windings, PCB windings are comprised of large numbers of copper traces, which are typically straight and without complex transposition. Eddy current loss in PCB traces can be estimated by 2D or 3D FE models, as described, for example, in [13], [17], [20].

For coreless machines, the eddy current loss needs to be considered during the design and optimization stage. However, the calculation of eddy current loss in conductors, including Litz wires and PCB traces, if solved directly using FE solvers, is time-consuming and challenging for large-scale design optimizations [21]. This paper proposes to use a hybrid analytical–numerical approach that can be directly incorporated into the multi-objective optimization algorithm to quickly estimate the eddy current loss in windings based on the variation of average flux density in equivalent macro coils from 3D transient FEA.

Based on the guidelines from Section II, the wire gauge for each strands needs to be at least AWG 38. A Litz wire consisting of 100 strands of AWG 40 magnet wires was selected, which is expected to be able to reduce the ac winding losses for this study to negligible levels. The equivalent macro coil model for Litz wire windings is illustrated in Fig. 2.

Assuming that all the conductors in coils are straight and directly exposed to a uniform magnetic field varying sinusoidally with time, neglecting the eddy current loss in end coils, the eddy current loss in Litz wire windings with round conductors

TABLE I
OPTIMIZATION VARIABLES AND THEIR RANGES.

| Variable | Description | Min. | Max. |
|---|---|---|---|
| $R_{ir}$ | Inner radius of rotor [mm] | 80 | 120 |
| $k_{cw}$ | Coil width / Max. coil width | 0.50 | 0.95 |
| $k_{ry}$ | Rotor yoke thickness / PM axial length | 0.5 | 1.5 |
| $k_s$ | Stator axial length / PM axial length | 0.5 | 2.0 |

is estimated by:

$$P_{eddy} = \sigma L_c N_c N_t N_s \omega^2 \frac{B_a^2 \pi d^4}{128}, \quad (1)$$

where $\sigma$ is the conductivity of conductors, $\omega$ the electrical angular velocity, $L_c$ the length of conductors, $N_c$ the number of coils, $N_t$ the number of turns per coil, $N_s$ the number of strands per turn, $d$ the diameter of each strand (conductor). $B_a$ is the amplitude of the flux density [9].

For PCB stator windings, the traces are treated as rectangular wires, and the equation for eddy current loss estimation is:

$$P_{eddy} = \sigma L_c N_c N_t N_s \omega^2 \frac{(B_{az}^2 w^2 + B_{a\phi}^2 h^2) wh}{24}, \quad (2)$$

where $B_{az}$ and $B_{a\phi}$ are the axial and tangential components of the flux density, and $w$ and $h$ are the width and height of each strand, respectively.

## IV. PARAMETRIC MODELING AND OPTIMIZATION

The material properties and dimensions of magnets and Litz wires are kept constant during the optimization since they are predetermined by available suppliers. The dimensions of the stator and rotor back iron are optimized to achieve the minimum total axial length and total electromagnetic loss, including the dc winding loss, ac winding loss and PM eddy current loss. The width and height of equivalent macro coils are $m$ and $n$ times the diameter of Litz wire for Litz wire windings, where $m$ and $n$ are positive integers. They can be equal or unequal. In PCB stator windings, the width and height of the equivalent macro coil are controlled similarly to keep the fill factor constant.

Four independent variables are identified for the optimization, as tabulated in Table I. The geometry of the coreless machine using Litz wire and PCB stator windings is illustrated in Fig. 3. The fill factor for equivalent macro coils is determined by the wire layout. It is 0.386 and 0.303 for the Litz wire winding and PCB stator winding shown in Fig. 2, respectively.

The optimization method is a variation of the 2-level surrogate-assisted algorithm which combines the multi-objective differential evolution (DE) and kriging meta-models to accelerate the generation of the Pareto front [22]. This optimization algorithm requires a reduced number of design evaluations and can be implemented in powerful workstations or high performance computing systems, enabling the accurate performance calculation of each candidate design in less than 10 minutes.

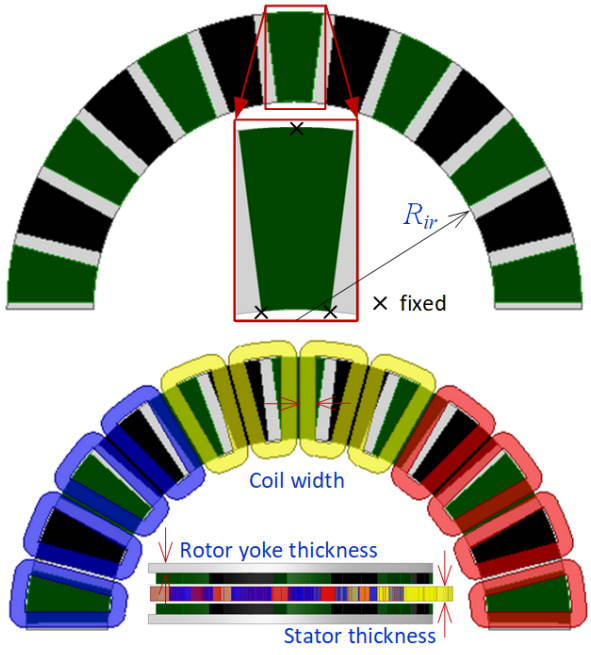


Fig. 3. Parametric 3D model and main geometric variables.

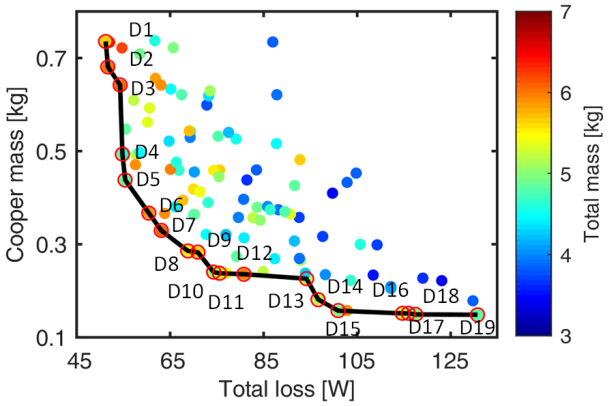


Fig. 4. The Pareto front and all the other designs evaluated by 3D FEA throughout the differential evolution for the 3-phase AFPM with fractional-slot concentrated windings.

## V. RESULTS AND DISCUSSION

The Pareto front for the optimization and all the other designs using Litz wires are shown in Fig. 4. The highest electromagnetic efficiency achieved by the optimum designs from the Pareto front is 98.8%. The box plot as shown in Fig. 5 indicates that independent variables of all the Pareto front designs are within their ranges and the optimization is acceptable. The ac winding loss accounts for a small fraction of the total electromagnetic loss, as shown by the loss breakdown in Fig. 6.

The PCB version is also optimized following the same procedure except the Litz wires are replaced by rectangular copper traces. The equation used for ac winding loss estimation and fill factor are changed according to the different constructions. One design example with PCB stator windings

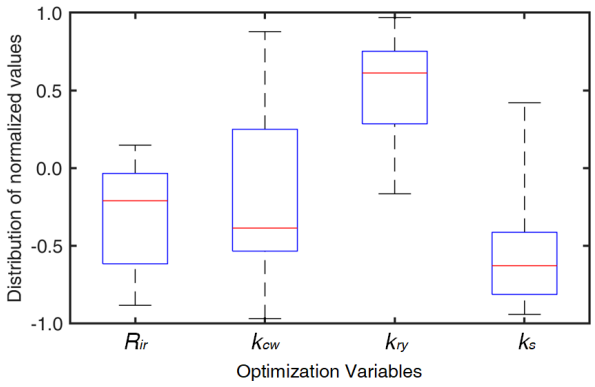


Fig. 5. Box plot for the Pareto front shown in Fig. 4.

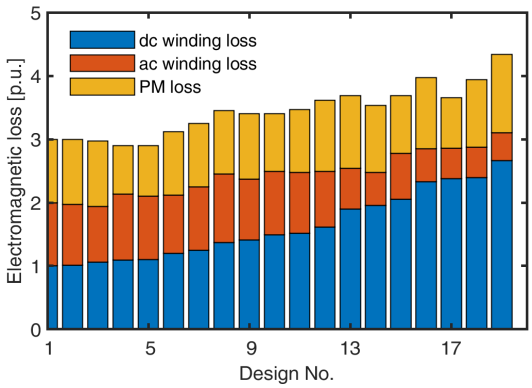


Fig. 6. The loss breakdown of Pareto front designs shown in Fig. 4. The three loss components are normalized relative to the values for the Design 1.

from the optimization was selected and modeled in detail, as shown in Fig. 7. There are two PCBs, one for each phase, stacked with a phase shift of 90 electrical degrees. Each PCB has 6 layers with 50 traces per layer. The terminals are shown in the zoomed-in view in Fig. 7a.

## VI. Prototyping and Testing

Three selected optimal designs are being fabricated. The customized test fixture shown in Fig. 8 is able to adjust the airgap length during the testing. The structure developed has been constructed using tight tolerance aluminum jig plate and a 20 mm keyed steel shaft, as well as a dual bearing system for proper alignment. This design allows flexibility for mounting of various AFPM machines and precise calibration of their airgaps. The fixture is also equipped with a vertical back plate with an opening for the shaft such that an encoder can be mounted for speed feedback to be used in the control loop for the machine.

To assemble the coreless machine under test to the fixture, the first of the two rotors is mounted to a flanged clamping shaft collar and then placed onto the shaft into position and locked into place using the collar's locking nuts. Nylon spacers are then bolted to the vertical plate of the fixture, which the stator is then bolted to. This procedure sets the airgap between the first rotor and stator. To combat axial forces

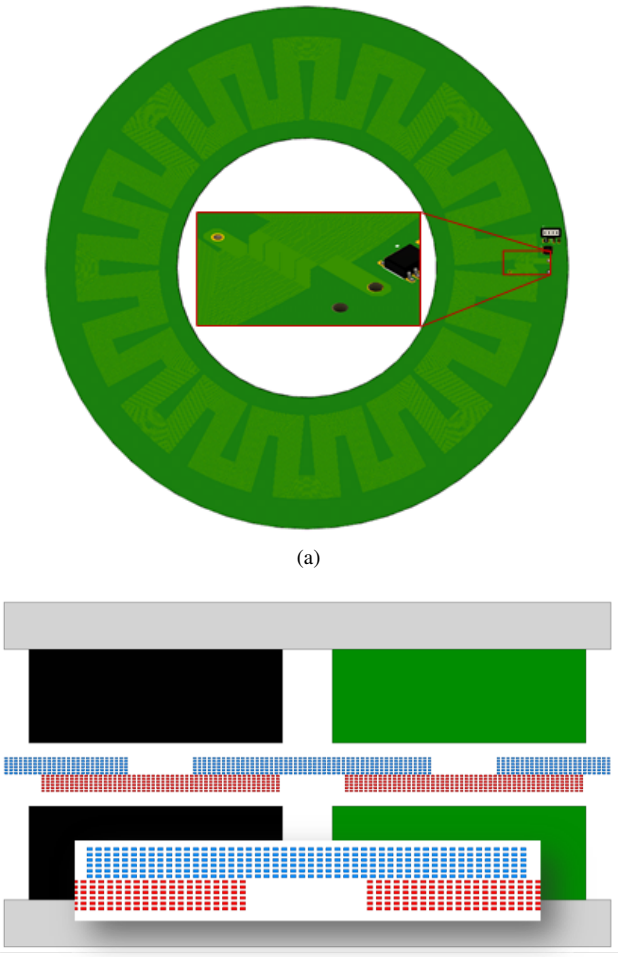

(a)

(b)

Fig. 7. Detailed modeling of a PCB stator design example, (a) top view, (b) unrolled 2D view from a cylindrical cut plane shown together with rotors.

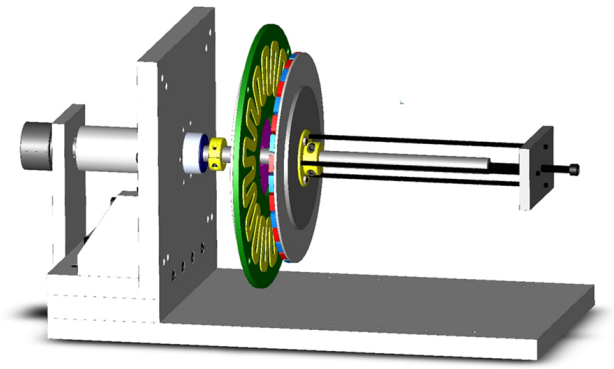

Fig. 8. Customized test fixture with the coreless machine with PCB stator installed.

present between the second rotor and stator, an adjustment tool is used which allows precise, controlled placement of the second rotor on the shaft. Once the airgap is satisfactory, the second rotor is locked into place using the same flanged shaft collar approach as the first.

## VII. Conclusion

Coreless AFPM machines have special constructions and their windings can be designed with additional degrees of freedom as there are no geometrical constraints imposed by teeth and slots. Such machines may achieve very high efficiency by employing Litz wire or PCB windings and through design optimization.

Three coreless AFPM machines, two with Litz wire windings and the other with PCB stator windings, were optimized taking into account the ac winding loss by the proposed optimization procedure. It is shown that high efficiency can be achieved through the proposed design optimization method. The prototyping of three selected designs are underway, with testing and experimental validations to follow.

## Acknowledgment

The support of the National Science Foundation, NSF Grant #1809876, of University of Kentucky, the L. Stanley Pigman endowment and ANSYS Inc., is gratefully acknowledged.

## References

[1] N. Taran, V. Rallabandi, G. Heins, and D. M. Ionel, "Coreless and conventional axial flux permanent magnet motors for solar cars," *IEEE Trans. Ind. App.*, vol. 54, no. 6, pp. 5907–5917, Nov 2018.

[2] V. Rallabandi, N. Taran, and D. M. Ionel, "Multilayer concentrated windings for axial flux pm machines," *IEEE Trans. on Magn.*, vol. 53, no. 6, pp. 1–4, 2017.

[3] V. Rallabandi, N. Taran, D. M. Ionel, and J. F. Eastham, "Coreless multidisc axial flux pm machine with carbon nanotube windings," *IEEE Trans. Magn.*, vol. 53, no. 6, pp. 1–4, 2017.

[4] N. Taran, V. Rallabandi, and D. M. Ionel, "Waved: A coreless axial flux pm motor for drive systems with constant power operation," in *2019 IEEE Trans. Electric Mach. Conf. and Expo (ITEC)*, 2019, pp. 1–6.

[5] M. G. Kesgin, P. Han, N. Taran, and D. M. Ionel, "Overview of flywheel systems for renewable energy storage with a design study for high-speed axial-flux permanent-magnet machines," in *2019 8th Int. Conf. Renew. Ener. Research and App. (ICRERA)*, 2019, pp. 1026–1031.

[6] Z. Zhang, A. Matveev, R. Nilssen, and A. Nysveen, "Ironless permanent-magnet generators for offshore wind turbines," *IEEE Trans. Ind. Appl.*, vol. 50, no. 3, pp. 1835–1846, 2014.

[7] B. Xia, J. Shen, P. C. Luk, and W. Fei, "Comparative study of air-cored axial-flux permanent-magnet machines with different stator winding configurations," *IEEE Trans. Ind. Electron.*, vol. 62, no. 2, pp. 846–856, 2015.

[8] Y. Liu, Z. Zhang, C. Wang, W. Geng, and T. Yang, "Design and analysis of oil-immersed cooling stator with non-overlapping concentrated winding for high-power ironless stator AFPM machines," *IEEE Trans. Ind. Electron.*, Mar. 2020, DOI: 10.1109/TIE.2020.2978694.

[9] N. Taran, V. Rallabandi, D. M. Ionel, G. Heins, and D. Patterson, "A comparative study of methods for calculating ac winding losses in permanent magnet machines," in *2019 IEEE Int. Electric Mach. Drives Conf. (IEMDC)*, 2019, pp. 2265–2271.

[10] N. Taran and D. M. Ionel, "A hybrid analytical and fe-based method for calculating ac eddy current winding losses taking 3d effects into account," in *2019 IEEE Energy Conv. Cong. and Expo. (ECCE)*, 2019, pp. 4867–4872.

[11] C. Zwyssig, S. D. Round, and J. W. Kolar, "An ultrahigh-speed, low power electrical drive system," *IEEE Trans. Ind. Electr .*, vol. 55, no. 2, pp. 577–585, 2008.

[12] H. Hämäläinen, J. Pyrhönen, J. Nerg, and J. Talvitie, "AC resistance factor of Litz-wire windings used in low-voltage high-power generators," *IEEE Trans. Ind. Electron.*, vol. 61, no. 2, pp. 693–700, 2014.

[13] F. Marignetti, G. Volpe, S. M. Mirimani, and C. Cecati, "Electromagnetic design and modeling of a two-phase axial-flux printed circuit board motor," *IEEE Trans. Ind. Electron.*, vol. 65, no. 1, pp. 67–76, 2018.

[14] X. Wang, C. Li, and F. Lou, "Geometry optimize of printed circuit board stator winding in coreless axial field permanent magnet motor," in *IEEE Veh. Power Prop. Conf. (VPPC)*, 2016, pp. 1–6.

[15] D. Gambetta and A. Ahfock, "Designing printed circuit stators for brushless permanent magnet motors," *IET Electr. Power Appl.*, vol. 3, no. 5, pp. 482–490, 2009.

[16] Elektrisola, [Online]. Available: https://www.elektrisola.com/en/hf-litz-wire-litz/products/terminology-basics/selection-of-litz-wire - parameters.html.

[17] N. S., S. P. Nikam, S. Singh, S. Pal, A. K. Wankhede, and B. G. Fernandes, "High-speed coreless axial-flux permanent-magnet motor with printed circuit board winding," *IEEE Trans. Ind. Appl.*, vol. 55, no. 2, pp. 1954–1962, 2019.

[18] T. Guillod, J. Huber, F. Krismer, and J. W. Kolar, "Litz wire losses: Effects of twisting imperfections," in *IEEE Workshop Contr. Modeling Power Electron. (COMPEL)*, 2017, pp. 1–8.

[19] C. R. Sullivan, "Computationally efficient winding loss calculation with multiple windings, arbitrary waveforms, and two-dimensional or three-dimensional field geometry," *IEEE Trans. Power Electron.*, vol. 16, no. 1, pp. 142–150, 2001.

[20] X. Wang, W. Pang, P. Gao, and X. Zhao, "Electromagnetic design and analysis of axial flux permanent magnet generator with unequal-width PCB winding," *IEEE Access*, vol. 7, pp. 164 696–164 707, 2019.

[21] M. Rosu, P. Zhou, D. Lin, D. M. Ionel, M. Popescu, F. Blaabjerg, V. Rallabandi, and D. Staton, *Multiphysics Simulation by Design for Electrical Machines, Power Electronics and Drives*. Wiley-IEEE Press, 2017.

[22] N. Taran, D. M. Ionel, and D. G. Dorrell, "Two-level surrogate-assisted differential evolution multi-objective optimization of electric machines using 3-D FEA," *IEEE Trans. Magn.*, vol. 54, no. 11, pp. 1–5, 2018.